

Impact of inhomogeneous diffusion on secondary cosmic ray and antiproton local spectra

Álvaro Tovar-Pardo^{a,b} Pedro De La Torre Luque^{a,b,c} Miguel A. Sánchez-Conde^{a,b}

^aInstituto de Física Teórica UAM-CSIC, Universidad Autónoma de Madrid, C/ Nicolás Cabrera, 13-15, 28049 Madrid, Spain

^bDepartamento de Física Teórica, M-15, Universidad Autónoma de Madrid, E-28049 Madrid, Spain

^cThe Oskar Klein Centre, Department of Physics, Stockholm University, AlbaNova SE-10691 Stockholm, Sweden

E-mail: atovarpar@gmail.com, pedro.delatorre@uam.es, miguel.sanchezconde@uam.es

Abstract. Recent γ -ray and neutrino observations seem to favor the consideration of non-uniform diffusion of cosmic rays (CRs) throughout the Galaxy. In this study, we investigate the consequences of spatially-dependent inhomogeneous propagation of CRs on the fluxes of secondary CRs and antiprotons detected at Earth. A comparison is made among different scenarios in search of potential features that may guide us toward favoring one over another in the near future. We also examine both the influence of inhomogeneous propagation in the production of secondary CRs from interactions with the gas, and the effects of this scenario on the local fluxes of antiprotons and light antinuclei produced as final products of dark matter annihilation. Our results indicate that the consideration of an inhomogeneous diffusion model could improve the compatibility of the predicted local antiproton flux with that of B, Be and Li, assuming only secondary origin of these particles. In addition, our model predicts a slightly harder local antiproton spectrum, making it more compatible with the high energy measurements of AMS-02. Finally, no significant changes are expected in the predicted local flux of antiprotons and antinuclei produced from dark matter among the different considered propagation scenarios.

Contents

1	Introduction	1
2	Cosmic-ray propagation models	3
2.1	Simulation setup	3
3	Predictions from the uniform and spatial-dependent propagation setups	6
3.1	Impact on secondary nuclei and antinuclei production	6
3.1.1	Combined fits in the inhomogeneous setup	9
3.2	Impact on possible dark matter signals at Earth	10
4	Discussion and conclusions	11
A	Other observables in the best-fit inhomogeneous model	13
B	Antinuclei predictions	14

1 Introduction

Over the last century, cosmic rays (CRs) have proven to be a powerful tool for the study of multiple areas in physics, from Galactic astrophysics [1–3] to high-energy physics [4, 5]. Foremost, the indirect search for dark matter (DM) through the detection of CRs has recently emerged as a promising field [6, 7]. Additionally, the current interest shown by the scientific community in the field has increased in recent years thanks to the data provided by modern detectors, mainly, the AMS-02 experiment [8]¹, which showcases an unprecedented level of precision in its data in the energy range of GeV-TeV per nucleon.

Accelerated mainly in Supernova Remnants (SNRs), primary CRs (charged particles produced in the Big Bang Nucleosynthesis or in the stellar interior) travel along the Galaxy being deflected by the Galactic magnetic fields, interacting acollisionally with turbulent plasma waves and producing secondary particles by spallation phenomena with the gas present in the interstellar medium (ISM). Primary and secondary CRs eventually reach the Earth, allowing us to study, among others, the diffusive models that characterize their transport [9], the Galactic environment or, ultimately, the nature of DM particles and the morphology of the structures they form [10].

The widely embraced scientific perspective holds that CRs primarily follow a diffusive pattern of motion along our Galaxy, stemming from their interactions with magnetohydrodynamical waves [11, 12]. The exchange of energy with these waves causes the reacceleration and deflection of a CR. All the diffusive behavior of CRs is enclosed in the so-called diffusion coefficient, which was found to follow a power law in rigidity with a spectral index δ [13, 14],

$$D(\rho) \sim D_0 \beta^\eta \left(\frac{\rho}{\rho_0} \right)^\delta \quad (1.1)$$

where β is the speed of the particles in units of speed of light and η is an exponent fitted to the data. Both the normalization constant, D_0 , and the spectral index are values that

¹<https://ams02.space/>

have to be obtained experimentally. Measured spectra lead to typical local values of $\delta \approx 0.50$ [12], and a normalization constant in the order of $D_0 \sim (3 - 5) \times 10^{28} \text{ cm}^2 \text{ s}^{-1}$ at $\rho \sim 1 \text{ GV}$ [15]. The most widely used observable to determine the diffusion parameters is the secondary-to-primary flux ratio, which depends almost exclusively on the diffusion parameters and the effective cross-section of secondary production. Hence, cross section values play a fundamental role in the evaluation of the diffusion coefficient. Usually the high uncertainties associated with the effective cross-section affect both the determination of diffusion parameters and the identification of possible DM annihilation signals. For instance, cross section uncertainty associated with boron or antiproton production can be up to 20% [16–18].

On top of this, it is unclear if the spectral behavior of the diffusion coefficient is equal in the whole Galaxy or if, on the contrary, it is only valid for our local neighbourhood. In other words, whether diffusion occurs uniformly or if it exhibits a spatial dependence is a fundamental open problem [19, 20]. At present, most (if not all) analyses of CRs employ a diffusion coefficient that is uniform across the Galaxy. Nevertheless, there are indications suggesting that this may not necessarily be the case. The Milky Way exhibits non-homogeneous density of matter and magnetic fields, being proved that there are more structures and astrophysical activity in the Galactic center (GC) [21]. Therefore, it is expected that the diffusion of CRs in the GC differs from that in our solar neighbourhood. Notably, the Fermi Large Area Telescope (*Fermi*-LAT), on board the NASA Fermi satellite [22] has performed observations indicating a discernible increase in the GeV γ -rays diffuse flux directed towards the GC [23–27]. Furthermore, recent data on γ -ray emissions at the PeV [28, 29] and neutrino emissions at the TeV-PeV range, as disclosed by the IceCube experiment [30], have revealed an unexpectedly elevated flux. This phenomenon can be adequately elucidated by postulating that the propagation of CRs is not uniform across the Galaxy. For instance, recent studies [31, 32] has offered a natural explanation for the excesses found in the diffuse γ -ray emission by introducing a non-homogeneous diffusive model in CR transport, wherein a spatially-dependent spectral index is taken into account.

Additionally, this can be essential in searches of DM using CRs. The WIMP (Weakly Interactive Massive Particles) model posits the existence of DM particles capable of producing particle-antiparticle pairs with energies on the order of the GeV [33, 34]. In this regard, the measurement of antiparticles, such as antiprotons and antinuclei, could provide clear signals of WIMP annihilation due to their very low backgrounds, e.g., [16]. Finding DM signals requires a highly accurate model of the transport of CRs: a thorough understanding of CRs spectra is necessary for the subsequent detection of anomalies in the data.

This study explores the production of CRs in our Galaxy considering a spatially-dependent inhomogeneous diffusion model, and emphasizing its effect on the production of secondary CRs and antiprotons. The aim of this study is to demonstrate the impact that more realistic propagation setups have in the predicted fluxes of secondary CRs at Earth, yet we note that a full evaluation of the uncertainties related to inhomogeneous propagation setups is still far from being achievable. In Section 2, we outline the main motivations for this work, providing a concise discussion of the CRs transport models and the considered setup. Section 3.1 presents a comparison of the predicted local spectra of secondary CRs and antiprotons for the propagation scenarios considered. First, we examine a homogeneous transport model, treating it as the benchmark scenario for subsequent comparative studies with non-uniform models. Then, we analyze the results obtained with the inhomogeneous model from Ref. [31] and perform a combined fit to AMS-02 data. The results indicate that we can not distinguish between both scenarios with the current data, although inhomogeneous transport characterized by a

spatially-dependent spectral index could alleviate some existing tensions. In Section 3.2, we study the antiproton flux produced by DM annihilation for various WIMP masses and discuss the impact of neglecting the spatial dependence of the diffusion coefficient in current indirect DM searches. We discuss our findings and conclude in Section 4.

2 Cosmic-ray propagation models

As discussed above, the validity of the local spectral shape of CRs in different parts of the Galaxy is a fundamental open problem that has been actively studied over the past decade. Both, theoretical expectations and recent data suggest that the diffusion coefficient is not constant throughout the Galaxy [19, 28–30, 35]. In particular, a recent model [31, 32] implements a spectral index of the diffusion coefficient that depends on the distance from the GC to explain the hardening of the Galactic diffuse γ -ray flux observed by Fermi-LAT [36, 37], and takes the following form:

$$\delta(r) = \delta_0 \cdot r + \delta_1, \quad (2.1)$$

where δ_0 , δ_1 are parameters that can be determined through fits to the diffuse γ -ray data and r is the distance from the GC.

Physically, the adoption of this non-uniform expression for the diffusion coefficient leads to a higher CR confinement towards the GC (i.e., CRs stay in those zones for longer time, resulting in higher probability of interactions with the ISM and, therefore, more production of secondary particles). In this work, we adopt this parameterization of the spatial dependence of the diffusion coefficient and assess its implications in the current models describing local secondary CR data. Remarkably, the predicted CR flux close to the GC will be very different when assuming uniform and inhomogeneous CR diffusion (while it should not be very different at Earth since we adjust our models to reproduce the local CR data), as we show in Fig. 1 for H and He. Since the flux of local CR particles reflect their transport in the whole Galaxy, we expect secondary particles to show features of inhomogeneous transport.

While the ratios of secondary-to-primary CR fluxes (such as B/C, Be/O, etc), that are used to determine the propagation parameters, are expected to show small deviations (larger as energy increases) with the inhomogeneous model employed here, the antiproton flux and the antiproton-to-proton ratio (similarly for antinuclei, such as antideuteron and antihelium) could be expected to show larger differences, due to the fact that their flux at a given energy is mainly produced from (around 6 times) higher energy protons, where the effect of the spatially-dependent propagation setup is more relevant.

For the same reasons, it is worth exploring the scenario of inhomogeneous propagation in the context of the signals expected at Earth from DM production of antiprotons and antinuclei. Considering that most of the DM is concentrated at the GC, one may expect the DM-induced antiproton spectrum to be different in this diffusive scenario. Yet, in order to reveal anomalies in the antiproton data that could indicate the presence of DM signals, it will be mandatory to pay particular attention to the uncertainties in our predictions because of the diffusion setup employed, which is commonly the uniform diffusion scenario.

2.1 Simulation setup

To simulate the production and arrival of CRs, we solve the full transport equation (Eq. 2.2), for each CR species i , with the DRAGON2² code. This code solves numerically the transport

²https://github.com/cosmicrays/DRAGON2Beta_version

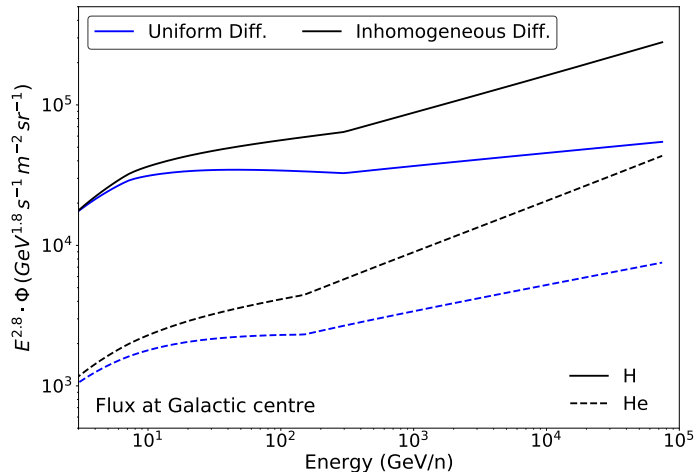


Figure 1: Comparison of the predicted flux of H and He for the inhomogeneous and uniform diffusion models evaluated at the GC.

equation within a realistic Galactic environment, yielding solutions of high reliability. For more details about the code, theory and treatment of the transport equation [38, 39].

$$\begin{aligned}
 -\vec{\nabla} \cdot (D\vec{\nabla}N_i + \vec{v}_\omega N_i) + \frac{\partial}{\partial p} \left[p^2 D_{pp} \frac{\partial}{\partial p} \left(\frac{N_i}{p^2} \right) \right] - \frac{\partial}{\partial p} \left[\dot{p} N_i - \frac{p}{3} (\vec{\nabla} \cdot \vec{v}_\omega) N_i \right] = \\
 = Q + \sum_{i < j} \left(c\beta n_{gas} \sigma_{j \rightarrow i} + \frac{1}{\gamma\tau_{j \rightarrow i}} \right) N_j - \left(c\beta n_{gas} \sigma_i + \frac{1}{\gamma\tau_i} \right) N_i
 \end{aligned} \tag{2.2}$$

This equation describes the propagation of CRs in the Galaxy for a given species i with density $N_i(\vec{r}, p)$. The left-hand-side of the equation describes the diffusive phenomenology (enclosed in the spatial diffusion coefficient, D , and D_{pp} in momentum space), as well as the convective processes and energy losses along the path of a CR. The right-hand-side takes into account the sources of injection of CRs for the species i , being Q the differential energy flux of primary CRs in units of $\text{m}^{-2}\text{s}^{-1}\text{sr}^{-1}\text{GV}^{-1}$, followed by nuclear fragmentation by interaction with the ISM gas (with $Z_j > Z_i$) and lately plausible annihilations of species i or decay into other states.

For the simulations performed in this study, the Galaxy is modeled as a cylinder with azimuthal symmetry and a radius of 30 kpc. Regarding the effective halo size (H, the effective height of the Galactic region where CRs diffuse), we set it to the value obtained in Ref. [40] from analysis of beryllium isotopes (^{10}Be), i.e., $H=4.72$ kpc. In our simulations, we inject the primary CRs ^1H , ^4He , ^{12}C , ^{14}N , ^{16}O , ^{20}Ne , ^{24}Mg , ^{28}Si , whose injection is adjusted to reproduce AMS-02 measurements [41–44]. This source injection is parameterized as a doubly broken power-law:

$$Q_{source} = \begin{cases} k_1 \times \left(\frac{E}{E_0} \right)^{\gamma_1} & \text{if } E < E_1 \\ k_2 \times \left(\frac{E}{E_0} \right)^{\gamma_2} & \text{if } E \in [E_1, E_2] \\ k_3 \times \left(\frac{E}{E_0} \right)^{\gamma_3} & \text{if } E > E_2 \end{cases} \tag{2.3}$$

where $\gamma_{1,2,3}$ are the injection parameters, $k_{1,2,3}$ normalization constants of the flux, and $E_{1,2}$ the rigidity breaks, with $E_1 = 8.0$ GV. $E_2 = 300$ GV. The spatial distribution of sources in the Galaxy is taken from Ref. [45].

The arrival of CRs in the solar environment is subject to the phenomenological conditions of the heliosphere. The Sun follows periods of cyclic activity that vary with time, mainly affecting the flux of low-energy CRs ($\lesssim 50$ GeV/n) passing through the heliosphere [16, 46]. Solar modulation is parameterized through a modification of the Force-Field approximation [47, 48], derived in Ref. [49],

$$\phi^\pm(t, R) = \phi_0(t) + \phi_1^\pm(t)F(R/R_0), \quad (2.4)$$

where we set the values of $\phi_0 = 0.61$ GV, $\phi_1 = 0.90$ GV and R_0 to 1 GV, based on analyses from Ref. [40] and [50].

We will take, as benchmark scenario for the homogeneous model, the diffusion parameters obtained in Ref. [40], from fits to the AMS-02 fluxes of the primary CRs mentioned above, the ratios of secondaries to primaries (B, Be, Li to C, O) and the antiproton-over-proton ratio, as well as the $^{10}\text{Be}/\text{Be}$ and $^{10}\text{Be}/^9\text{Be}$ ratios from various experiments – ACE [51], IMP [52, 53], ISEE [54], ISOMAX [55], Ulysses [56] and Voyager [57] missions – (see Ref. [58] for a recent analysis finding similar results). Our setup neglects the high energy break in the diffusion coefficient that was included in Ref. [40] in order to avoid more freedom and degenerate parameters in our evaluations. Instead, we include a break at high energies in the spectra of primary CRs (Eq. 2.3). We have verified that including this break in the diffusion coefficient only changes the predicted antiproton-over-proton spectrum by a roughly constant normalization factor of 1 – 2%, and the spectrum of B, Be and Li only above ~ 150 GeV. In this way, the diffusion parameters employed for the (benchmark) homogeneous diffusive model are $\delta = 0.49$, $D_0 = 4.49 \times 10^{28}$ cm²s⁻¹, $\eta = -0.91$ and Alfvén speed of $V_A = 13.06$ km/s. These analyses also consider, as nuisance parameters, scaling factors to adjust the normalization of spallation cross sections of secondary nuclei, whose values are compatible with the uncertainties that currently exist [18]. In particular, the scale factors in our benchmark model, for B, Be, Li and \bar{p} are, respectively, $\mathcal{S}_B = 0.99$, $\mathcal{S}_{Be} = 0.92$, $\mathcal{S}_{Li} = 0.88$, $\mathcal{S}_{\bar{p}} = 1.11$, similar to what is found by the recent analyses of Ref. [59]. The values of main parameters employed are provided in Table 1, for each of the propagation setups described in the text.

Then, we consider the inhomogeneous model, evaluated from the diffuse γ -ray observations by Fermi-LAT, as discussed above, henceforth referred to as γ -*inhomogeneous*, for comparison with the predictions from the uniform diffusion scenario. The γ -inhomogeneous model adopts the parameterization of the spectral index found from γ -ray observations by Ref. [31], which has the following form:

$$\delta(r) = 0.04 \cdot r + 0.17 \quad (2.5)$$

In this case, we keep the same value for the halo height, V_A , η and scaling factors, as in the benchmark (homogeneous) scenario, and adjust only the normalization of the diffusion coefficient to fit the B/C ratio from AMS-02 data. The injection spectra of primary CRs is also reevaluated (to reproduce AMS-02 observations) to avoid biasing the results. This allows us to directly compare the impact of such inhomogeneous diffusion setup in the production of secondary CRs (and, specially, in the local antiproton spectrum). The main propagation parameters employed are summarized in Table 1, which contains a third model that is explained below (Sec. 3.1.1).

We particularly focus our attention to the B/C and \bar{p}/p flux ratios. Unlike boron, that forms from spallation interactions of heavy CRs, antiprotons are produced by inelastic collisions of primary particles, being p-p reactions the dominant production channel with

$\sim 60\%$ contribution to the \bar{p} spectrum [60]. An important kinematical consequence of the different mechanisms of creation of these secondary CRs is that, while B will roughly inherit the same energy per nucleon as the parent nucleus, antiprotons will be produced at energies much smaller (around a factor of 6) than the parent protons [61]. Therefore, one could expect larger deviations in the predicted \bar{p}/p ratio, from the inhomogeneous scenario, than in the B/C ratio. Further, non-annihilating inelastic reactions of the type $p + \bar{p} \rightarrow \bar{p}' + X$ (being X some residual particles) are also allowed, henceforth referred to as tertiary antiprotons, which will be more relevant at low energies. Antinuclei are similarly produced [62], although in much lower amounts, and we will also discuss how their production can change in the different scenarios. Another source of antiprotons and antinuclei production could be DM annihilation [58, 63, 64], which is explored in Section 3.2.

	$D_0 [10^{28} \text{ cm}^2 \text{ s}^{-1}]$	δ	\mathcal{S}_B	\mathcal{S}_{Be}	\mathcal{S}_{Li}	$\mathcal{S}_{\bar{p}}$
Homogeneous	4.43	0.49	0.99	0.96	0.92	1.11
γ-inhomogeneous	4.83	$0.04 \cdot r + 0.17$	0.99	0.96	0.92	1.11
Inhomogeneous best-fit	4.55	$0.04 \cdot r + 0.20$	1.00	0.97	0.93	1.02

Table 1: Main parameters characterizing the propagation models considered in this work. The normalization and spectral index of the diffusion coefficient, D_0 and δ , respectively, are displayed in the central columns, while the scale factors of the cross-section for secondary nuclei are presented in the right columns, \mathcal{S}_B , \mathcal{S}_{Be} , \mathcal{S}_{Li} , $\mathcal{S}_{\bar{p}}$. The rest of propagation parameters are the same in all the scenarios and their values are provided in the main text of Section 2.

3 Predictions from the uniform and spatial-dependent propagation setups

3.1 Impact on secondary nuclei and antinuclei production

In this section, we compare the predicted secondary fluxes (production from CR interactions with the interstellar gas) obtained from the uniform scenario with those obtained from the γ -inhomogeneous model. In particular, we focus on the B/C and \bar{p}/p ratios. The predicted ratios are compared to AMS-02 data in Fig. 2 for the homogeneous diffusion scenario (top panels) and γ -inhomogeneous model (bottom panels). Residuals are shown in the bottom panel, defined as (model–data)/data throughout the work, where ‘model’ denotes the predictions obtained via simulation.

Regarding the B/C spectra, we compare the modeled, unmodulated spectrum with Voyager-1 data [65] in the MeV/n energy range, and the modulated spectrum with AMS-02 data in the GeV/n–TeV/n range. In the GeV/n range, we observe that the predictions are compatible with AMS-02 data within a $\sim 5\%$ in both scenarios, although we observe that above 100 GeV/n the predicted spectrum in the homogeneous scenario tends to differ more significantly from the data. This has been one of the main arguments motivating the addition of a break in the diffusion coefficient (theoretically explained as a change of turbulence regime [66]) that allows to fit better the secondary-to-primary ratios above a hundred GeV. We remark that in the γ -inhomogeneous scenario the statistical preference for such a break will be less significant, as can be seen from the residuals. However, we observe that, although

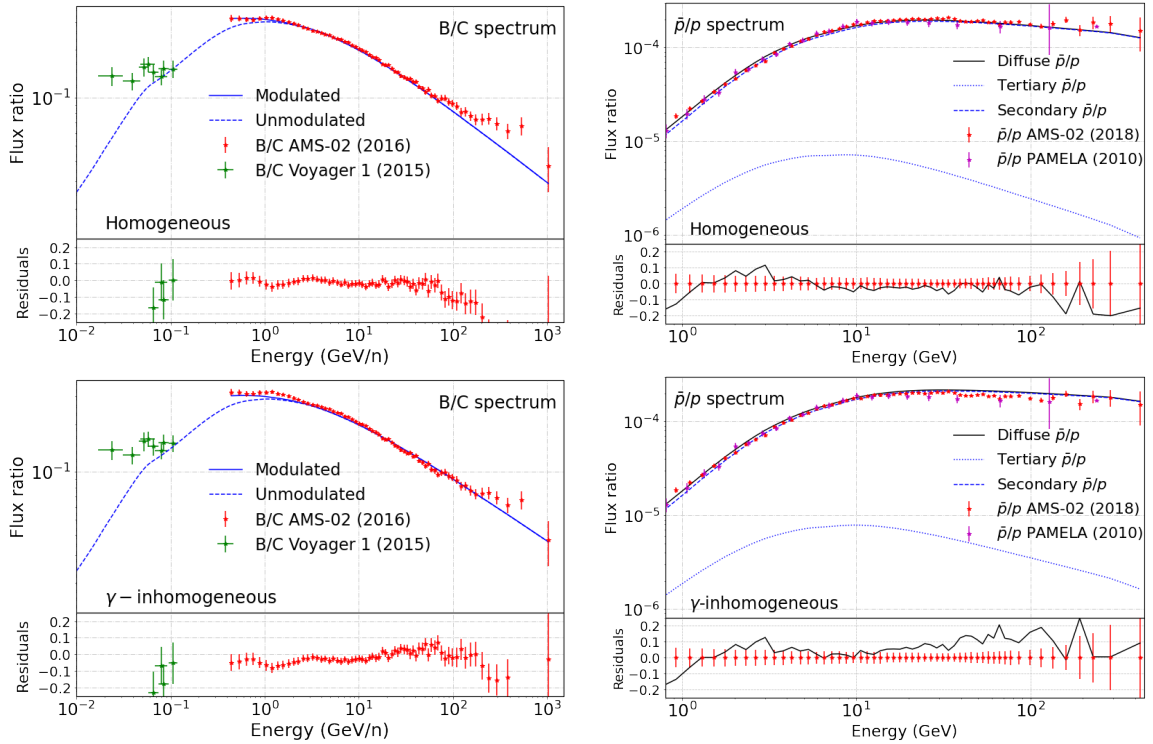


Figure 2: Left panels: B/C flux ratios as measured by AMS-02 (red) and Voyager 1 (green), in comparison with our model predictions (blue lines). **Right panels:** \bar{p}/p flux ratios as measured by AMS-02 (red) and PAMELA (magenta), in comparison with our model predictions (blue lines). The predictions for the diffusive homogeneous model are shown in the top panels and those from the γ -inhomogeneous in the bottom panels. Residuals are defined as (model–data)/data.

the predicted B/C ratio in the γ -inhomogeneous scenario appears compatible with the 1σ uncertainties in AMS-02 data, the predicted trend of the spectrum seems slightly harder than the one observed in the data.

Regarding the \bar{p}/p spectrum, we observe that the predicted ratio in the homogeneous scenario seems to follow a quite similar trend to that from AMS-02 data, showing very flat residuals. Moreover, above around 100 GeV, the predicted antiproton spectrum seems slightly softer than that from AMS-02 data. This does not improve adding a high-energy break in the diffusion coefficient and has been observed in the past, motivating the proposal of different mechanisms to explain this disagreement in the trends [67, 68]. Note, though, that it is not a statistically significant issue, given the uncertainty in antiproton data at those energies. In turn, the \bar{p}/p flux ratio obtained from γ -inhomogeneous model clearly reveals a spectrum that deviates significantly from AMS-02 measurements, with a discrepancy that grows as energy gets higher. In particular, the predicted \bar{p}/p ratio in this scenario shows a higher discrepancy with respect to the trend measured by AMS-02 than in the B/C ratio. This diffusion scenario entails, therefore, a substantial increase in the production of antiprotons. For the sake of a fair comparison, modulation parameters as well as cross sections scale factors are the same as in the homogeneous scenario. In fact, what we appreciate is not only a larger production of antiprotons, but a remarkable change in the shape of the spectrum, particularly

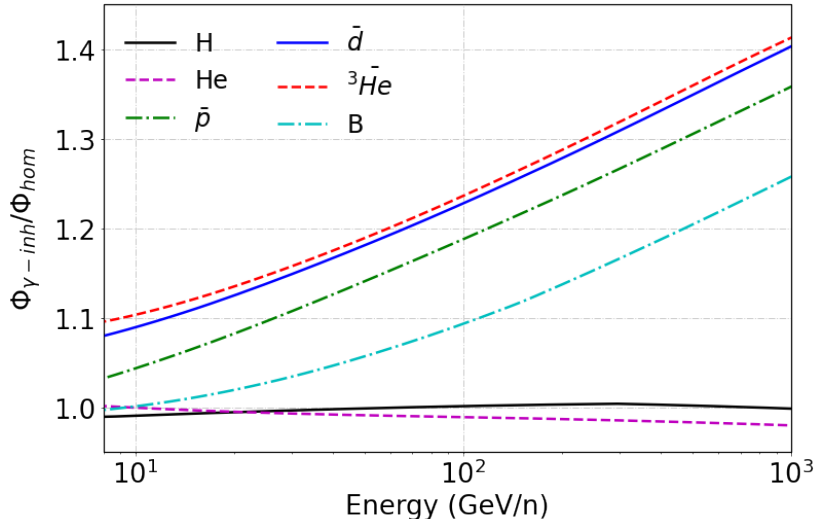


Figure 3: Ratios of the predicted fluxes at Earth between the γ -inhomogeneous diffusive model and the homogeneous model, for different nuclei depicted in the legend.

at high energies. It is important to notice that modifying the scale factors for antiproton cross sections could get our prediction in the γ -inhomogeneous scenario closer to the data, but yet the trend of the spectrum and the data will still be very different and incompatible with the measurements.

To facilitate the comparison of the differences between the considered diffusive models in the production of secondary CRs, we illustrate the ratio with energy between both scenarios in Fig. 3 up to 1 TeV/n for protons, He, B, \bar{p} , \bar{d} and ${}^3\bar{He}$ nuclei. We find that the production of secondary nuclei increases substantially in the γ -inhomogeneous model, predicting a harder trend of the spectrum. For instance, the predicted B flux is about 10% greater than in the homogeneous case at 100 GeV/n. Concerning antinuclei, fluxes of \bar{p} , \bar{d} , ${}^3\bar{He}$ are around 20% greater than in the homogeneous case at 100 GeV/n. This larger increase of secondary antiprotons and antinuclei with respect to B is due to the fact that the spectrum of antiprotons at this energy is mainly produced by protons of much higher energies, where the differences from the inhomogeneous and homogeneous scenarios become more significant. The heavier the antinuclei, the larger deviation due to the kinematics of the interactions producing them (\bar{d} are mainly produced by protons with energy around 15 times higher, and ${}^3\bar{He}$ is mainly formed from protons around 30 times more energetic).

These comparisons also indicate that although uncertainties in the determination of the spatial dependence of the diffusion coefficient can be relevant in our predictions of CR spectra at Earth, cross section uncertainties on the production of secondary CRs are still the leading factor of uncertainty³, not allowing us to really distinguish between these propagation models with any accuracy.

³For CR secondary nuclei and antiprotons, these uncertainties are often evaluated to be around 20%, and even higher above tens of GeV, due to the lack of experimental data. For antinuclei, the lack of measurements do not allow us to have a robust estimation and different evaluations agree usually within a factor of 2 for \bar{d} and at least a factor of a few for ${}^3\bar{He}$.

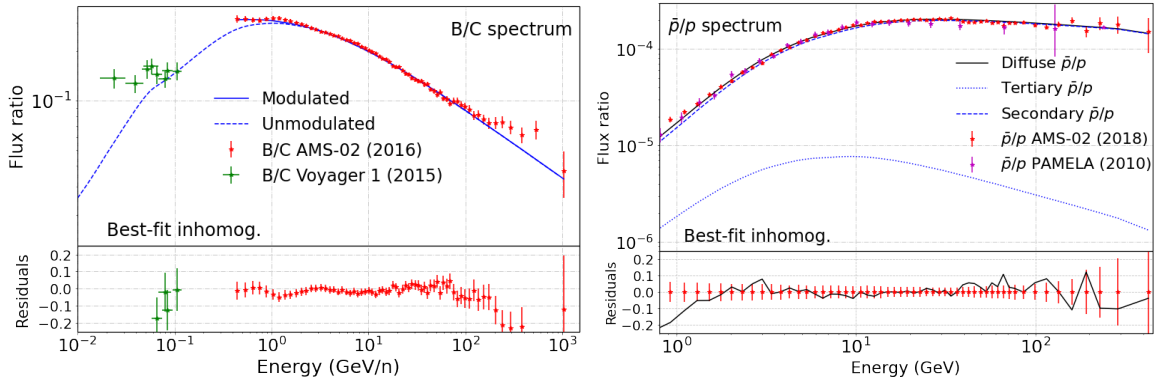


Figure 4: **Left panel:** B/C flux ratio measured by AMS-02 (red) and Voyager 1 (green), in comparison with the prediction from our Best-fit inhomogeneous diffusion model (blue lines). **Right panel:** \bar{p}/p flux ratio measured by AMS-02 (red) and PAMELA (magenta) compared with that predicted from best-fit inhomogeneous diffusion model. Residuals are defined as $(\text{model} - \text{data})/\text{data}$.

3.1.1 Combined fits in the inhomogeneous setup

Given that the γ -inhomogeneous model seems to predict spectra whose trend for the B/C and \bar{p}/p ratios do not exactly follow that from AMS-02 data (specially for the \bar{p}/p ratio, the predicted spectrum seems considerably harder; see bottom left panel of Figure 2), we address here if an overall reproduction of the B, Be, Li and \bar{p} species can be achieved simultaneously with the kind of inhomogeneous model that we are using. In particular, we adjust the spectra of these species through the simultaneous fit of the propagation and injection parameters to AMS-02 data, leaving fixed the δ_0 parameter (see Eq. 2.1), since it is obtained from γ -ray diffuse observations, as well as the η and V_A parameters. Therefore, we let free in the fit the D_0 and δ_1 (which regulates the δ value at Earth position), as well as the scale factors for the cross sections of these secondary CRs. This fit allows us to reproduce the AMS-02 data accurately, as shown in Fig. 4 for the \bar{p}/p (right panel) and B/C (left panel) ratios, as well as for the rest of CRs (see Fig. 7 in Appendix A). The obtained best-fit parameters obtained are given in Table 1. We also show the predicted secondary spectra of \bar{d} , ${}^3\bar{H}e$ in Appendix B, compared to current upper limits and sensitivities of future detectors.

Two main conclusions can be derived from our analysis of the *best-fit* γ -inhomogeneous model:

- The combined fit in the inhomogeneous scenario leads to a best-fit scaling of the antiproton cross sections of 2%, much smaller than the 11% scale needed in the homogeneous case (rightmost column of Table 1). This means that this scenario significantly reduces the tension in the predicted grammage needed to reproduce the antiproton spectrum with respect to the grammage needed to reproduce the group of B, Be and Li.
- We observe that the antiproton spectrum (and the \bar{p}/p ratio) gets slightly harder, as observed before. This may alleviate the fact, also commented above, that the high energy part of the predicted antiproton spectrum seems softer than that observed by AMS-02, making again more compatible the predictions from B, Be, Li and \bar{p} in the scenario where only secondary production is assumed.

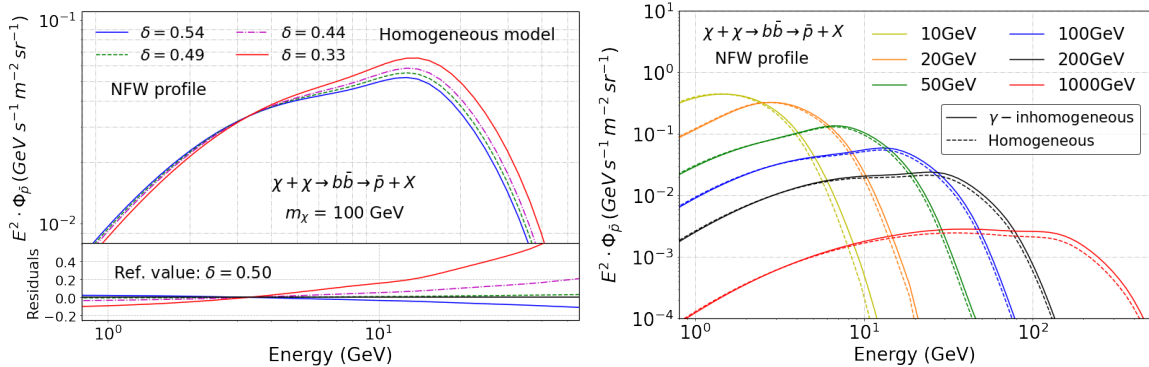


Figure 5: Left panel: Impact on \bar{p} production from DM annihilation for different effective spectral indices in the homogeneous propagation model. Residuals are taken as $(\text{model} - \text{ref.model}) / \text{ref.model}$, where ref.model is the flux obtained with $\delta = 0.5$. **Right panel:** Comparison of the predicted \bar{p} flux from DM annihilation for various WIMP masses in different propagation scenarios. The solid lines represent the flux predicted by the γ -inhomogeneous model, while the dashed lines represent those from the homogeneous model. The annihilation rate is set to $\langle \sigma v \rangle = 2.33 \cdot 10^{-26}$ cm³/s, i.e., the thermal relic value [74]. In both panels we adopt an NFW profile [75] for the DM distribution in the Galaxy.

Concretely, we observe that the predicted local B spectrum only increases by $\sim 3\%$ at 100 GeV with respect to the benchmark homogeneous diffusion setup, while the local \bar{p} spectrum changes up to a 7 – 8% at this energy (see Fig. 8 in App. A). Given that the uncertainties in the current data above 100 GeV are still high, it is not possible to find clear indications favoring any scenario and it would be too premature to state that this kind of inhomogeneous model makes our predicted antiproton spectrum from secondary production significantly more compatible with that of B, Be and Li compared to predictions from a homogeneous model. A recent work [59] reached a similar conclusion when analyzing other kinds of inhomogeneous setups. We do observe that this kind of inhomogeneous scenario, motivated by diffuse γ -ray observations, can offer a simple and realistic explanation for the tensions discussed above, and that future data on secondary CRs at higher energies could lead to more robust indications favoring a concrete propagation scenario. In general, we observe that different kind of inhomogeneous models proposed in the literature (see e.g. Refs.[69–71]) lead to a predicted \bar{p} spectrum more compatible with AMS-02 data than homogeneous models. This could indicate a common trait: models that predict a proton spectrum slightly harder than locally outside our local neighborhood are favored by the current \bar{p} local measurements.

3.2 Impact on possible dark matter signals at Earth

In this section we explore the impact that the different considered diffusion setups may have in the production of antiprotons from the annihilation of DM particles. The DM particle, χ , can annihilate producing $b\bar{b}$ quarks which eventually decay into other hadrons, producing antiprotons as a final result ($\chi + \chi \rightarrow b\bar{b} \rightarrow \bar{p} + X$). Even though other annihilation channels are kinematically available [72, 73], we take $b\bar{b}$ as the reference channel hereafter. We stress that a different annihilation channel would affect equally the predicted spectra in both scenarios, since it changes only the spectrum at production, leaving unchanged our conclusions.

As one would expect, the measured antiproton flux on Earth is sensitive to the parameters of the transport model. Different diffusion parameters will therefore provide different DM

signals. As we have discussed throughout the work, a different spectral index indicates that particles of different energies will diffuse for longer or shorter time in the Galaxy. Similarly, if one considers the γ -inhomogeneous model (Eq. 2.1), which implies that particles spend longer times at the GC, it is expected that the effect in the DM signal at Earth would be equivalent to that predicted from a low effective spectral index (i.e., $\delta_{effective}^{inhom.} < \delta^{hom.}$). This reasoning gets even stronger given that the density of DM particles is expected to be higher in the GC. In the left panel of Figure 5, we show the predicted \bar{p} spectrum from DM annihilation in the homogeneous scenario, for different values of the spectral index, all of them plausible and consistent with the CRs transport theory. For instance, a variation of the effective spectral index of $\Delta\delta \approx 0.20$ changes the \bar{p} signal at Earth approximately by a factor of 2. In this exercise, we adopted the standard Navarro-Frenk-White density profile [75] for the distribution of DM in the Galaxy.

Hence, given the form of the spectral index considered in the inhomogeneous models, we expect a higher local flux of antiprotons and antinuclei from DM than in the homogeneous model. This is corroborated by Figure 5 (right), where we perform a comparison of the \bar{p} local flux obtained in the γ -inhomogeneous model with respect to the homogeneous scenario. WIMP masses of 10, 20, 50, 100, 200 and 1000 GeV are considered to annihilate to $b\bar{b}$ with a cross section equal to the thermal relic cross section, with value $\langle\sigma v\rangle = 2.33 \cdot 10^{-26}$ cm³/s [74]. A comparison of both models reveals that the local \bar{p} flux can be at most about 25% higher in the γ -inhomogeneous model at the peak of the emission. The discrepancy between the maximum flux produced by both models becomes more pronounced as the WIMP mass increases. In the range of WIMP masses between 10 and 100 GeV, the inhomogeneous models predict fluxes that are higher than those predicted in the homogeneous scenario by 1 – 10%. In addition, one would expect that these differences grow if we consider a more peaked DM density profile (more DM in the inner Galaxy), such as the contracted NFW (c-NFW), with slope of $\gamma = 1.2$, proposed to fit the Galactic center excess observed in γ -rays, see e.g., [23, 25].

We also evaluated the DM-induced local flux of antiprotons with the best-fit inhomogeneous scenario. What we found is that no important difference is found between the flux predicted in the homogeneous and best-fit inhomogeneous cases, for any of the DM masses explored. We illustrate this in Figure 6, where we consider two different DM density profiles: the NFW (left panel) and the c-NFW (right panel). In either case, the discrepancy in the antiproton flux between both models does not exceed 5%. This demonstrates that the constraints provided by local (secondary) CR data allow us to have a robust estimation of the DM-induced signals at Earth, regardless of how diffusion is in other places of the Galaxy. Yet, a larger family of inhomogeneous diffusion models must be explored to confidently establish this in every case.

4 Discussion and conclusions

In this study, we have examined the implications of assuming an inhomogeneous diffusion model of CR transport in the local flux of different secondary CRs in the GeV/n-TeV/n energy range, focusing on antiproton (\bar{p}) production and secondary nuclei. Given that the main information that we have from CRs is their local flux, the scientific community has predominantly explored uniform diffusion models to understand their propagation process. The main motivation to study an inhomogeneous transport model stems from recent results using neutrinos [30] and γ -rays [28, 29, 36], which have been shown to be successfully ex-

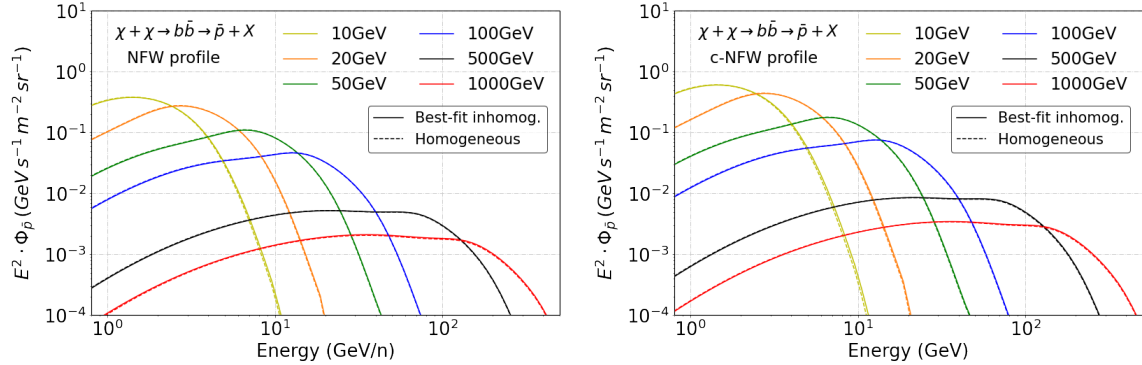


Figure 6: Comparison of the flux of antiprotons produced from DM annihilation for the case of adopting a NFW (left panel) and a c-NFW (right panel) DM density profile for the Galaxy, evaluated in the setup of uniform diffusion and with the best-fit setup of inhomogeneous diffusion.

plained through the adoption of a spatially-dependent diffusion coefficient [31, 32]. In this paper, we particularly focus on the differences between the predicted local flux of secondary CRs, antiprotons and antinuclei as given by homogeneous diffusion scenarios, and a class of inhomogeneous propagation model that considers a galactocentric radial dependence of the diffusion coefficient. This is investigated for both, their production in CR interactions with the ISM gas, and as products of DM annihilation (the latter only in the case of antiprotons and light antinuclei).

A general trait of inhomogeneous propagation models is that the slope of the spectrum of secondary CRs smoothly varies with energy (i.e., the spectrum is not a simple power-law), because different energies feature the propagation of CRs in different effective zones of the Galaxy (see, e.g., Ref. [69]). However, these changes may be arbitrarily small, as the inhomogeneous model explored here predicts. Therefore, we have conducted a direct comparison of the predictions from the homogeneous and inhomogeneous scenarios to understand what are the features that may lead us to disentangle between these scenarios. To achieve our goal, we have solved the full transport equation within a realistic Galactic, state-of-the-art environment using the DRAGON2 code. We first make sure to reproduce AMS-02, PAMELA and Voyager-1 experimental data of primary and secondary nuclei, and secondary-to-primary flux ratio, with simultaneous fits in each scenario to guarantee highly reliable and consistent models.

Regarding the secondary production of CRs, we find that the inhomogeneous model predicts a remarkably harder spectrum at Earth compared to the homogeneous propagation case, yet only marginally different to the one predicted by the homogeneous model in the GeV/n range once we adjust the model to reproduce simultaneously all the AMS-02 measurements (specially, the observations on secondary B, Be, Li and \bar{p}). However, we demonstrate that the production of secondary antiprotons is significantly more affected by inhomogeneous propagation (due to kinematical effects of the interactions producing them), leading to higher production at higher energies. In particular, the antiproton TeV flux predicted in this scenario would become significantly different to that expected in the homogeneous scenario. Therefore, should future data confirm the current hint – i.e., that the antiproton data seems to follow a harder trend than the one predicted in current (homogeneous) models – this could serve as an indication in favor of inhomogeneous propagation of CRs in the Galaxy. An additional point

favoring the inhomogeneous scenario is that we are able to achieve a very good simultaneous fit of B, Be, Li and \bar{p} almost without modifying the antiproton cross sections, while this simultaneous fit in the homogeneous scenario requires around a 10% scaling of the antiproton cross sections to reproduce all these species simultaneously.

We also investigate how this inhomogeneous diffusion model affects the predicted local flux from DM production of antiproton. We find that, although one could expect small variations on the predicted flux of these antiparticles at Earth, the current observations of secondary CRs by AMS-02 allow us to constrain these DM signals at Earth to be roughly the same in both scenarios (always lower than $\sim 5\%$ difference). We find that this is true even for a very peaked DM density profile for the Galaxy, such as the contracted NFW profile that fits the γ -ray Galactic center excess, and for a large range of DM masses that we test here (from ~ 10 GeV to ~ 1 TeV). Yet, we expect our current DM indirect searches with antiprotons must be affected, at least, by the expected secondary \bar{p} production. Although our results are based only in the $b\bar{b}$ channel, the same conclusions must hold for other channels too, given that changing to a different channel only affects the CR spectrum at the injection.

To end, we emphasize that the propagation of CRs in the Galaxy can be more complex than initially thought, and that different kind of inhomogeneous (and anisotropic) diffusion scenarios will result in different key features that could be tested with current and future CR experiments. Indeed, probably only a combination of different observables and messengers would allow us to improve our current description of the CR propagation processes in the Galaxy in the near future.

Acknowledgments

We thank Daniele Gaggero for useful discussions. P.D.L. has been supported by the European Research Council under grant 742104 and the Swedish National Space Agency under contract 117/19 and is currently supported by the Juan de la Cierva JDC2022-048916-I grant, funded by MCIU/AEI/10.13039/501100011033 European Union "NextGenerationEU"/PRTR. The work of P.D.L. and M.A.S.C. was supported by the grants PID2021-125331NB-I00 and CEX2020-001007-S, both funded by MCIN/AEI/10.13039/501100011033 and by "ERDF A way of making Europe". They also acknowledge the MultiDark Network, ref. RED2022-134411-T. This project used computing resources from the Swedish National Infrastructure for Computing (SNIC) projects 2021/3-42, 2021/6-326, 2021-1-24 and 2022/3-27 partially funded by the Swedish Research Council through grant no. 2018-05973.

A Other observables in the best-fit inhomogeneous model

We show in this appendix the fitted spectra of primary and secondary CRs in the best-fit inhomogeneous model, depicted in Table 1 and Section 3.1.1. In Figure 7, we illustrate the simulated spectra of p, He, C, N, O, Ne, Mg and Si (top panel) and the ratios of B, Be and Li to C and O (bottom panel), which are fitted to AMS-02 and PAMELA data in the GeV/n energy range. The fit of the primary nuclei provides the injection parameters for each species, according to Eq. 2.3. The fit to the secondary-to-primary flux ratios, along with the \bar{p}/p ratio, allows us to infer the diffusion parameters in agreement with experimental data.

In Figure 8, a comparison of nuclei and antinuclei fluxes is established between the best-fit inhomogeneous model and the homogeneous one. The first one predicts a production of secondary nuclei (B, Be, Li) approximately 15% higher than the homogeneous model at

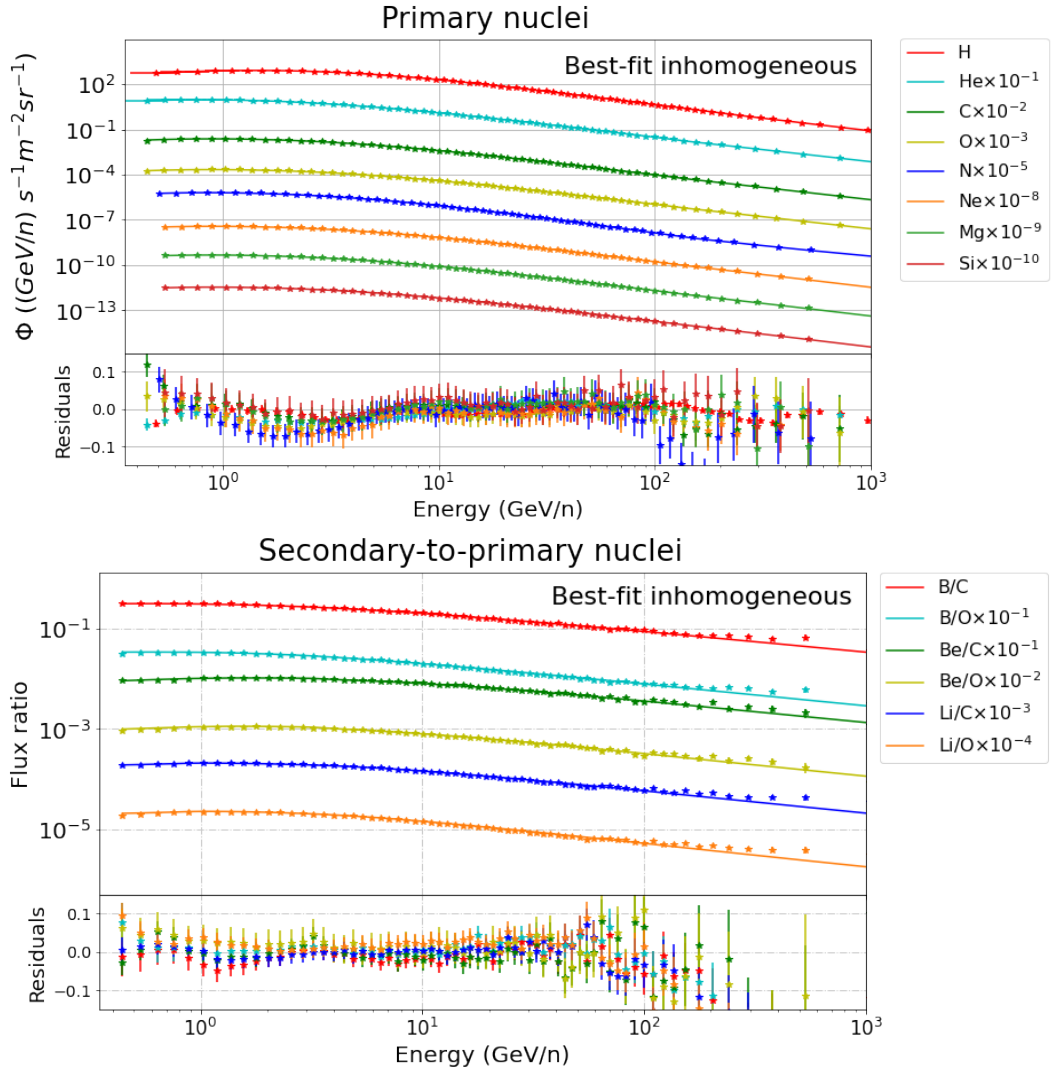


Figure 7: Upper panel: Primary nuclei spectra at Earth measured by AMS-02 (points) and predicted by the best-fit inhomogeneous model (solid line). **Lower panel:** Secondary-to-primary nuclei flux ratio at Earth measured by AMS-02 (points) and predicted by the best-fit inhomogeneous model (solid line). Residuals are defined as $(\text{model} - \text{data})/\text{data}$.

1 TeV/n, with an increase of about 20% for antiprotons and 30-35% for antideuterium and antihelium-3. Nevertheless, the production of secondaries decreases by approximately 10% compared to the γ -inhomogeneous model, with antiprotons flux being the most affected (from 35% down to 20%).

B Antinuclei predictions

In this appendix, we present and delve further into the details of antinuclei spectra. The full implementation of antinuclei production and propagation in the DRAGON2 code is described in Refs [62, 76]. In the context of the best-fit inhomogeneous model, we illustrate the predicted fluxes for antideuterium (\bar{d}) and antihelium-3 (${}^3\bar{He}$) in Figure 9. Antinuclei can be produced

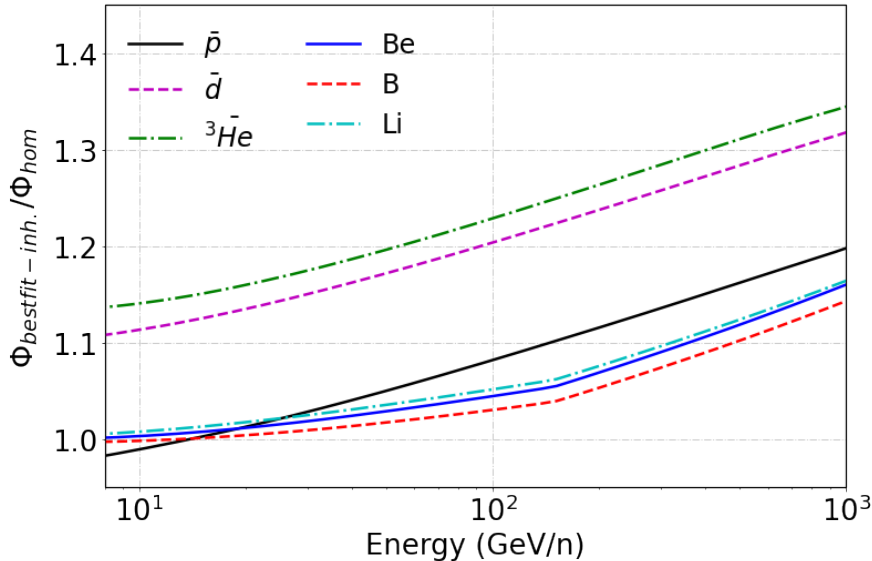


Figure 8: Comparison of the ratios of predicted CR fluxes at Earth from the best-fit inhomogeneous diffusive model and the homogeneous model, for secondary CR nuclei and antinuclei.

as secondary CRs (top panels) and as the end product of DM annihilation through the $b\bar{b}$ channel for NFW (middle panels) and c -NFW (bottom panels) DM density profiles. Currently, there are no experimental data available to contrast the predicted fluxes. In turn, we present the sensitivity bands of specific experiments that can detect such antinuclei. In the top panels of Fig. 9, we show the sensitivity regions for the RICH and TOF instruments in the AMS-02 detector (taken from Ref. [77]), for 15 years of operation, the upper-limits from the Balloon-borne Experiment with a Superconducting Spectrometer (BESS) [78], and the sensitivity region for the General AntiParticle Spectrometer (GAPS) [77, 79] (for the expected three flights of 35 days, each). Moreover, we include the forecasted sensitivity for the future Antimatter Large Acceptance Detector In Orbit (ALADInO) [80] (expected for 5 years of operation). According to our results, we do not foresee $^3\bar{H}e$ to be detected by AMS-02 in the next years. In turn, 1-4 GeV/n \bar{d} are likely to be captured by AMS (RICH). To compare the differences between these diffusion models in secondary antinuclei fluxes, see Figure 8. Excitingly, ALADInO is expected to be able to resolve and measure with high precision the secondary flux of \bar{d} and $^3\bar{H}e$, which will certainly allow us to improve our modelling of coalescence of antinucleons (See details in Ref. [62]).

The production of antinuclei solely coming from DM annihilation follows a trend similar to that discussed for antiprotons in Section 3.2. In both NFW and c -NFW profiles (middle and bottom panels of Fig. 9, respectively), we find that the variations do not exceed 5% in the spectral peaks in any case, occasionally resulting in the antinuclei flux of the homogeneous model being slightly higher. This occurs in the case of $m_\chi \in [10-50]$ GeV, where the flux in inhomogeneous diffusion is 3% lower than the homogeneous one. We observe a barely noticeable increase in flux in the c -NFW profile compared to the NFW profile, approximately in the range of 1-2%. It is in the spectral peaks of $m_\chi \in [500-1000]$ GeV where the best-fit inhomogeneous model is larger over the homogeneous one, with an increase between models of about 2-3%.

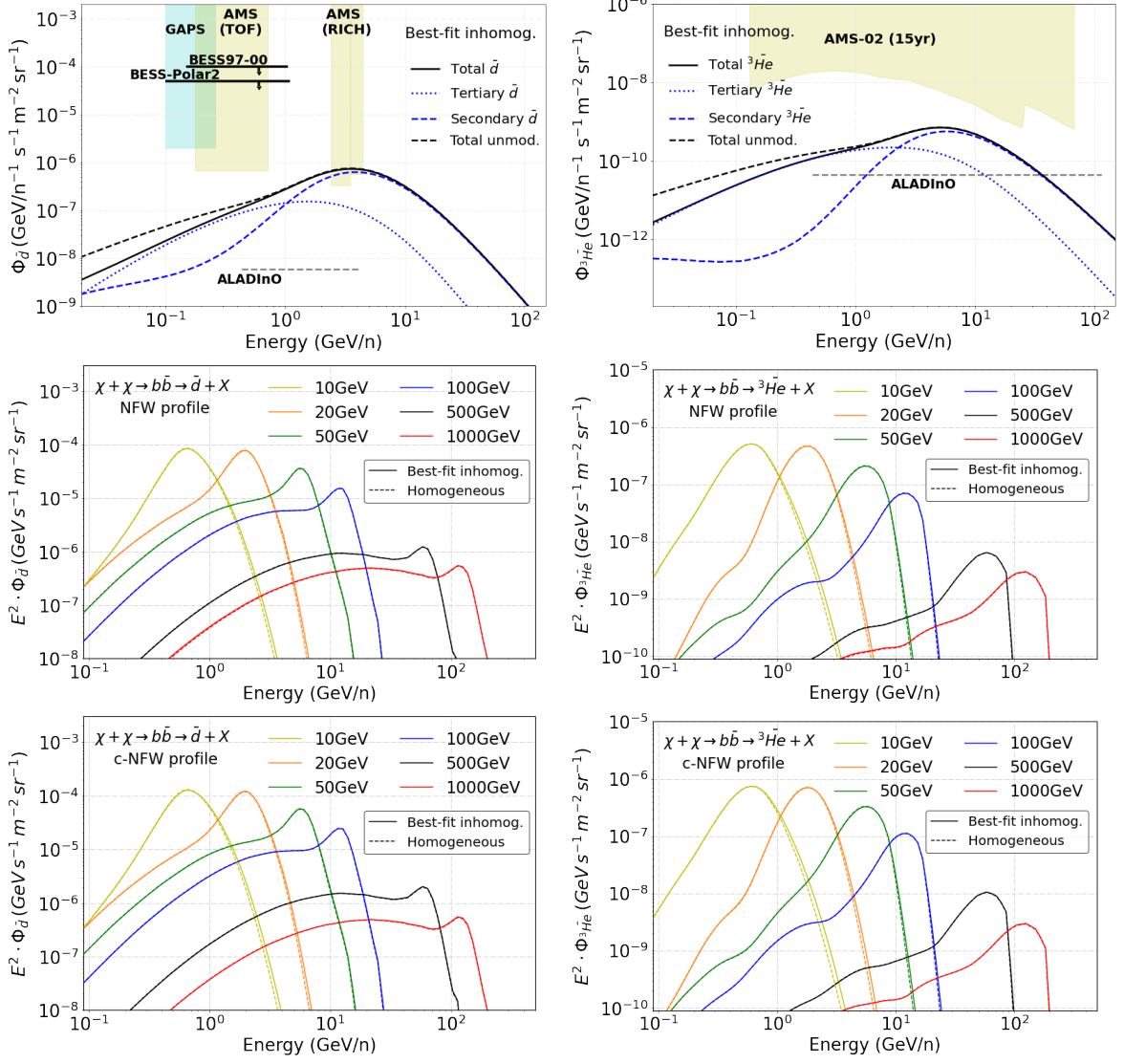


Figure 9: Top panels: Secondary antinuclei \bar{d} , ${}^3\bar{He}$ predicted fluxes with sensitivity bands of future experiments. No ${}^3\bar{He}$ from CR interactions is expected to be measured in the near future, whereas 1-4 GeV/n \bar{d} enter in the sensitivity domain of AMS (RICH). **Middle and bottom panels:** \bar{d} , ${}^3\bar{He}$ predicted fluxes within best-fit inhomogeneous model (solid line) from DM annihilation for NFW (central panels) and c-NFW (bottom panels) profiles compared to the fluxes predicted within the homogeneous model (dashed line). No differences higher than 3% in flux are obtained between both models at the spectral peaks. In most cases, solid lines overlap dashed lines.

References

- [1] A. Widmark, M. Korsmeier, and T. Linden, *Physical Review Letters* **130** (2023), [10.1103/physrevlett.130.161002](https://doi.org/10.1103/physrevlett.130.161002).
- [2] M. Ruszkowski and C. Pfrommer, “Cosmic ray feedback in galaxies and galaxy clusters – a pedagogical introduction and a topical review of the acceleration, transport, observables, and

- dynamical impact of cosmic rays,” (2023), [arXiv:2306.03141 \[astro-ph.HE\]](#) .
- [3] V. A. Semenov, A. V. Kravtsov, and D. Caprioli, *The Astrophysical Journal* **910**, 126 (2021).
- [4] C. E. Fichtel and J. Linsley, *Astrophysical Journal* **300**, 474 (1986).
- [5] T. K. Gaisser, *Cosmic Rays and Particle Physics* (1991).
- [6] J. Conrad and O. Reimer, *Nature Physics* **13**, 224–231 (2017).
- [7] F. Donato, *Physics of the Dark Universe* **4**, 41 (2014), dARK TAUP2013.
- [8] M. Aguilar *et al.* (AMS Collaboration), *Phys. Rev. Lett.* **110**, 141102 (2013).
- [9] A. W. Strong and I. V. Moskalenko, *The Astrophysical Journal* **509**, 212 (1998).
- [10] V. L. Ginzburg and S. I. Syrovatskii, *Topics in Astrophysics and Space Physics, New York: Gordon and Breach, 1969* (Gordon & Breach Publishing Group, 1969).
- [11] O. Fornieri, D. Gaggero, S. S. Cerri, P. De La Torre Luque, and S. Gabici, *Monthly Notices of the Royal Astronomical Society* **502**, 5821–5838 (2021).
- [12] P. Blasi and E. Amato, *Journal of Cosmology and Astroparticle Physics* **2012**, 010 (2012).
- [13] D. Maurin, R. Taillet, F. Donato, P. Salati, A. Barrau, and G. Boudoul, “Galactic cosmic ray nuclei as a tool for astroparticle physics,” (2002), [arXiv:astro-ph/0212111 \[astro-ph\]](#) .
- [14] E. Amato and P. Blasi, *Advances in Space Research* **62**, 2731 (2018), [arXiv:1704.05696 \[astro-ph.HE\]](#) .
- [15] A. W. Strong, I. V. Moskalenko, and V. S. Ptuskin, *Annual Review of Nuclear and Particle Science* **57**, 285 (2007), <https://doi.org/10.1146/annurev.nucl.57.090506.123011> .
- [16] P. von Doetinchem *et al.*, *Journal of Cosmology and Astroparticle Physics* **2020**, 035 (2020).
- [17] P. De La Torre Luque, M. Mazziotta, F. Loparco, F. Gargano, and D. Serini, *Journal of Cosmology and Astroparticle Physics* **2021**, 099 (2021).
- [18] Y. Génolini, D. Maurin, I. V. Moskalenko, and M. Unger, *Phys. Rev. C* **98**, 034611 (2018).
- [19] B. Schroer, O. Pezzi, D. Caprioli, C. C. Haggerty, and P. Blasi, *Monthly Notices of the Royal Astronomical Society* **512**, 233 (2022), <https://academic.oup.com/mnras/article-pdf/512/1/233/42894576/stac466.pdf> .
- [20] A. Dundovic, O. Pezzi, P. Blasi, C. Evoli, and W. H. Matthaeus, *Physical Review D* **102** (2020), [10.1103/physrevd.102.103016](https://doi.org/10.1103/physrevd.102.103016).
- [21] S. Gabici, C. Evoli, D. Gaggero, P. Lipari, P. Mertsch, E. Orlando, A. Strong, and A. Vittino, *Int. J. Mod. Phys. D* **28**, 1930022 (2019), [arXiv:1903.11584 \[astro-ph.HE\]](#) .
- [22] W. B. Atwood *et al.*, *The Astrophysical Journal* **697**, 1071–1102 (2009).
- [23] T. F. L. Collaboration, *The Astrophysical Journal* **840**, 43 (2017).
- [24] T. Daylan, D. P. Finkbeiner, D. Hooper, T. Linden, S. K. Portillo, N. L. Rodd, and T. R. Slatyer, *Physics of the Dark Universe* **12**, 1 (2016).
- [25] F. Calore, I. Cholis, and C. Weniger, *Journal of Cosmology and Astroparticle Physics* **2015**, 038–038 (2015).
- [26] K. N. Abazajian, N. Canac, S. Horiuchi, and M. Kaplinghat, *Physical Review D* **90** (2014), [10.1103/physrevd.90.023526](https://doi.org/10.1103/physrevd.90.023526).
- [27] D. Hooper and L. Goodenough, *Physics Letters B* **697**, 412–428 (2011).
- [28] M. Amenomori *et al.* (Tibet AS_γ Collaboration), *Phys. Rev. Lett.* **126**, 141101 (2021).
- [29] Z. Cao *et al.*, *Physical Review Letters* **131** (2023), [10.1103/physrevlett.131.151001](https://doi.org/10.1103/physrevlett.131.151001).

- [30] I. Collaboration, *Science* **380**, 1338 (2023), <https://www.science.org/doi/pdf/10.1126/science.adc9818> .
- [31] P. De La Torre Luque, D. Gaggero, D. Grasso, O. Fornieri, K. Egberts, C. Steppa, and C. Evoli, *Astronomy & Astrophysics* **672**, A58 (2023).
- [32] D. Gaggero, D. Grasso, A. Marinelli, A. Urbano, and M. Valli, *The Astrophysical Journal* **815**, L25 (2015).
- [33] L. Roszkowski, E. M. Sessolo, and S. Trojanowski, *Reports on Progress in Physics* **81**, 066201 (2018).
- [34] M. Kamionkowski, “Wimp and axion dark matter,” (1997), [arXiv:hep-ph/9710467 \[hep-ph\]](https://arxiv.org/abs/hep-ph/9710467) .
- [35] S. S. Cerri, D. Gaggero, A. Vittino, C. Evoli, and D. Grasso, *Journal of Cosmology and Astroparticle Physics* **2017**, 019–019 (2017).
- [36] M. Ackermann *et al.*, *The Astrophysical Journal* **750**, 3 (2012), [arXiv:1202.4039 \[astro-ph.HE\]](https://arxiv.org/abs/1202.4039) .
- [37] P. Lipari and S. Vernetto, *Phys. Rev. D* **98**, 043003 (2018).
- [38] C. Evoli, D. Gaggero, A. Vittino, G. D. Bernardo, M. D. Mauro, A. Ligorini, P. Ullio, and D. Grasso, *Journal of Cosmology and Astroparticle Physics* **2017**, 015 (2017).
- [39] C. Evoli, D. Gaggero, A. Vittino, M. D. Mauro, D. Grasso, and M. N. Mazziotta, *Journal of Cosmology and Astroparticle Physics* **2018**, 006 (2018).
- [40] P. D. L. T. Luque, *Journal of Cosmology and Astroparticle Physics* **2021**, 018 (2021).
- [41] M. Aguilar *et al.*, *Physics Reports* **894**, 1 (2021), the Alpha Magnetic Spectrometer (AMS) on the International Space Station: Part II - Results from the First Seven Years.
- [42] M. Aguilar *et al.* (AMS), *Phys. Rev. Lett.* **121**, 051103 (2018).
- [43] M. Aguilar *et al.* (AMS Collaboration), *Phys. Rev. Lett.* **119**, 251101 (2017).
- [44] M. Aguilar *et al.* (AMS Collaboration), *Phys. Rev. Lett.* **120**, 021101 (2018).
- [45] D. R. Lorimer, A. J. Faulkner, A. G. Lyne, R. N. Manchester, M. Kramer, M. A. McLaughlin, G. Hobbs, A. Possenti, I. H. Stairs, F. Camilo, M. Burgay, N. D’Amico, A. Corongiu, and F. Crawford, *Monthly Notices of the Royal Astronomical Society* **372**, 777 (2006), https://academic.oup.com/mnras/article-pdf/372/2/777/40676920/mnras_372_2_777.pdf .
- [46] A. W. Labrador and R. A. Mewaldt, *The Astrophysical Journal* **480**, 371 (1997).
- [47] M. S. Potgieter, *Living Reviews in Solar Physics* **10**, 3 (2013).
- [48] L. J. Gleeson and W. I. Axford, *The Astrophysical Journal letters* **149**, L115 (1967).
- [49] I. Cholis, D. Hooper, and T. Linden, *Phys. Rev. D* **93**, 043016 (2016), [arXiv:1511.01507](https://arxiv.org/abs/1511.01507) .
- [50] A. Reinert and M. W. Winkler, *JCAP* **01**, 055 (2018), [arXiv:1712.00002 \[astro-ph.HE\]](https://arxiv.org/abs/1712.00002) .
- [51] N. E. Yanasak *et al.*, *apj* **563**, 768 (2001).
- [52] M. Garcia-Munoz, G. M. Mason, and J. A. Simpson, *apj* **217**, 859 (1977).
- [53] M. Garcia-Munoz, J. A. Simpson, and J. P. Wefel, in *International Cosmic Ray Conference*, International Cosmic Ray Conference, Vol. 2 (1981) p. 72.
- [54] M. E. Wiedenbeck and D. E. Greiner, *apjl* **239**, L139 (1980).
- [55] T. Hams *et al.*, *ApJ* **611**, 892 (2004).
- [56] J. J. Connell, *apjl* **501**, L59 (1998).
- [57] W. Webber, A. Lukasiak, and F. McDonald, *ApJ* **568**, 210 (2002).
- [58] P. De la Torre Luque, M. W. Winkler, and T. Linden, Accepted in *JCAP* (2024), [arXiv:2401.10329 \[astro-ph.HE\]](https://arxiv.org/abs/2401.10329) .

- [59] M. D. Mauro, M. Korsmeier, and A. Cuoco, “Data-driven constraints on cosmic-ray diffusion: Probing self-generated turbulence in the milky way,” (2023), [arXiv:2311.17150 \[astro-ph.HE\]](#) .
- [60] P. d. l. T. Luque, *Cosmic-ray propagation and production of secondary particles in the Galaxy*, Ph.D. thesis, Bari U. (2020), [arXiv:2202.07063 \[astro-ph.HE\]](#) .
- [61] N. Tomassetti, *Physical Review D* **92** (2015), [10.1103/physrevd.92.081301](#).
- [62] P. De La Torre Luque, M. W. Winkler, and T. Linden, (2024), [arXiv:2404.13114 \[astro-ph.HE\]](#) .
- [63] F. Calore, M. Cirelli, L. DEROME, Y. Genolini, D. Maurin, P. Salati, and P. D. Serpico, *SciPost Physics* **12** (2022), [10.21468/scipostphys.12.5.163](#).
- [64] Y. Génolini, M. Boudaud, M. Cirelli, L. Derome, J. Lavalle, D. Maurin, P. Salati, and N. Weinrich, *Physical Review D* **104** (2021), [10.1103/physrevd.104.083005](#).
- [65] E. C. Stone, A. C. Cummings, F. B. McDonald, B. C. Heikkila, N. Lal, and W. R. Webber, *Science* **341**, 150 (2013).
- [66] P. Blasi, E. Amato, and P. D. Serpico, *Phys. Rev. Lett.* **109**, 061101 (2012).
- [67] I. Cholis, D. Hooper, and T. Linden, *Phys. Rev. D* **95**, 123007 (2017).
- [68] P. Mertsch, A. Vittino, and S. Sarkar, *Phys. Rev. D* **104**, 103029 (2021).
- [69] N. Tomassetti, *The Astrophysical Journal Letters* **752**, L13 (2012).
- [70] S. Recchia and S. Gabici, “On the origin of the spectral features observed in the cosmic ray spectrum,” (2023), [arXiv:2312.11397 \[astro-ph.HE\]](#) .
- [71] Y.-Q. Guo, Z. Tian, and C. Jin, *The Astrophysical Journal* **819**, 54 (2016).
- [72] M. Cirelli, G. Corcella, A. Hektor, G. Hütsi, M. Kadastik, P. Panci, M. Raidal, F. Sala, and A. Strumia, *Journal of Cosmology and Astroparticle Physics* **2011**, 051–051 (2011).
- [73] C. Arina, M. D. Mauro, N. Fornengo, J. Heisig, A. Jueid, and R. R. de Austri, “Cosmixs: Cosmic messenger spectra for indirect dark matter searches,” (2023), [arXiv:2312.01153 \[astro-ph.HE\]](#) .
- [74] G. Steigman, B. Dasgupta, and J. F. Beacom, *Physical Review D* **86** (2012), [10.1103/physrevd.86.023506](#).
- [75] J. F. Navarro, C. S. Frenk, and S. D. White, *Astrophys. J.* **462**, 563 (1996), [arXiv:astro-ph/9508025](#) .
- [76] P. De la Torre Luque, *PoS ICRC2023*, 1369 (2023).
- [77] T. Aramaki *et al.*, *Astroparticle Physics* **74**, 6 (2016).
- [78] K. Abe *et al.*, *Phys. Rev. Lett.* **108**, 131301 (2012).
- [79] F. Rogers *et al.*, “Sensitivity of the gaps experiment to low-energy cosmic-ray antiprotons,” (2022).
- [80] R. Battiston *et al.*, *Experimental Astronomy* **51**, 1299 (2021).